

SM EFT effects in Vector-Boson Scattering at the LHC

A. DEDES¹, P. KOZÓW², M. SZLEPER³

¹ *Department of Physics, Division of Theoretical Physics,
University of Ioannina, GR 45110, Greece*

² *Institute of Theoretical Physics, Faculty of Physics, University of Warsaw,
ul. Pasteura 5, 02-093 Warsaw, Poland*

³ *National Center for Nuclear Research, High Energy Physics Department,
ul. Pasteura 7, 02-093 Warsaw, Poland*

Abstract

The assumption that the Standard Model is an Effective Field Theory (SM EFT) of a more fundamental theory at a higher, than electroweak, energy scale, implies a growth of cross-sections for electroweak Vector Boson Scattering (VBS) processes signalling the appearance of a resonance (or resonances) nearby that scale. In this article, we investigate in detail SM EFT effects from dimension-6 operators in VBS with like-sign- W production in fully leptonic decay modes at the High Luminosity LHC (HL-LHC). We find that these effects are important for a handful of operators, most notably for the operator composed of three $SU(2)$ field strength tensors responsible for strong transversely polarized vector boson interactions. Current global fits on Wilson-coefficients allow for a signal immediately permissive at the HL-LHC if not accessible at the current LHC-dataset.

1 Introduction

It is widely believed that the Standard Model (SM) [1–3] is an Effective, low energy, Field Theory (EFT) approximation [4–6] to a more fundamental theory (UV-theory) which overtakes the SM at energies, at least several times, higher than the Electroweak (EW) scale. One of the very important processes that may shed light on the dynamics of the UV-theory is the electroweak Vector Bosons Scattering (VBS)¹. This claim is true because,

- (i) VBS processes are directly related to the mechanism of electroweak symmetry breaking, and as such, regarded as complementary to Higgs-boson measurements at LHC,
- (ii) although inaccessible directly, heavy particles, constituents of the UV-theory, may leave their trace in modifying the strength and dynamics of electroweak interactions, spoiling for example the, at most constant, center of mass energy (s)-behaviour of the SM $VV \rightarrow VV$ ($V = W^\pm, Z, \gamma$) amplitudes. In the SM EFT, this results in a growth of cross-sections at energies straight after the electroweak scale.

¹For a review see [7].

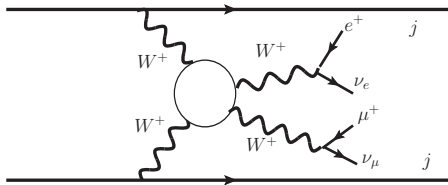


Figure 1: A Feynman diagram picturing a VBS process.

- (iii) In the SM, even when next-to-leading order corrections are included, VBS processes feature particularly slow slope with energy in comparison to other electroweak processes [8].

Therefore, points (ii) and (iii) imply potential sensitivity to the UV-theory particles, especially to those strongly interacting with EW-gauge bosons.

Unfortunately, there is no VV -collider available², however the $VV \rightarrow VV$ reactions are indirectly accessible at the LHC, particularly within its high luminosity phase (HL-LHC), through the process $pp \rightarrow 2\text{jets} + 2\text{lepton pairs}$. While all the elastic processes e.g. $ZZ, WZ, W^\pm W^\pm, W^\pm W^\mp$ have been extensively investigated at the LHC, the same-sign W^+W^+ process in fully-leptonic decay mode has been the first process to be observed³ at 5σ [12] (based on the 13 TeV dataset), and is currently confirmed at a sensitivity far above 5σ [11]. For that reason, in this paper we shall investigate in detail the VBS process through W^+W^+ -scattering, namely the reaction

$$pp \rightarrow 2\text{jets} + W^{+*} W^{+*} \rightarrow 2\text{jets} + 2\text{ charged-leptons} + 2\text{ neutrinos} .$$

This is exemplified by Fig. 1 of a particular final state. Throughout this work, we mostly focus on the HL-LHC experimental perspectives.

We follow the SM EFT approach⁴ in which the corrections from heavy and decoupled UV-states [14], can be parametrized by a number of i -indexed dimension-6 operators, Q_i , added to the SM Lagrangian, associated with dimensionless (or dimensionful) Wilson coefficients C^i (or f^i), as

$$\mathcal{L} = \mathcal{L}_{SM} + \sum_i \frac{C^i}{\Lambda^2} Q_i + \dots \equiv \mathcal{L}_{SM} + \sum_i f^i Q_i + \dots . \quad (1.1)$$

The mass scale Λ denotes the lightest mass among the heavy particle masses within the UV-theory. Although the EFT expansion in (1.1) is written up-to $1/\Lambda^2$, in one occasion below we will fill in the “...” with several dimension-8 operators where the dimensionless Wilson coefficients are suppressed by four powers of Λ 's.

The real advantage of the EFT approach follows from the fact that one can study the discovery potential of the physics Beyond the SM (BSM) without any knowledge of theories that may lay ahead by making use of a limited number of operators arranged order-by-order in $1/\Lambda$ expansion. More precisely, here we consider the SM EFT theory that matches UV-models featuring linearly realized electroweak symmetry breaking, where the Higgs field is part of the SM Higgs doublet. The SM EFT basis of non-redundant operators has been constructed first at dimension-6, commonly referred to as Warsaw basis [15], and very recently at dimension-8 [16, 17].

It is a common approach, in both experimental and theoretical literature, to use EFT for studying VBS channels as an indirect search for physics Beyond the Standard Model (BSM) [18–22];

²Interestingly in a certain setup, it has been argued that a muon collider could effectively be regarded as such [9,10].

³The actual measurement involves a sum of both W^+W^+ and W^-W^- processes; W^+W^+ makes about 4/5 of it [11].

⁴For a review see ref. [13].

for a recent review see [23]. The point of focus of such studies is usually the $VVVV$ quartic-couplings, i.e. the operators that modify Quartic Gauge Couplings (QGC) and simultaneously leave intact Trilinear Gauge Couplings (TGC) and Higgs-gauge boson interactions. In SM EFT such kind of physics arise from dimension-8 operators [24, 25] and, consequently, the searches are typically conducted as if there was no effect arising from dimension-6 operators. Here, we investigate the validity of this assumption, given experimental constraints on dimension-6 interactions (which necessarily modify TGC) emerging from independent channels, by studying in detail the like-sign W -boson production through VBS at (HL-)LHC. We would like to emphasise that the aim of this work is not to model accurately possible BSM signals, but to check which dimension-6 operators can produce non-negligible effect as allowed by the most up to date experimental constraints from non-VBS processes on the corresponding Wilson coefficients (including also the important issue of bounding background operators), which include new LHC Run 2 results. The numerical significance of dimension-6 operators in VBS has been pointed out in Ref. [26, 27].

Concerning the bounds on dimension-6 operators, we use the ones reported in Refs. [28] and [29] (non-4-fermion operators) and [30, 31] (4-fermion operators)⁵. In [28, 29], the truncation of EFT cross-sections is performed consistently at dimension-6, namely, no (dimension-6)² terms are considered, that would arise from squaring the (SM + dimension-6) amplitude. It is known that inclusion of the latter significantly improves the constraints from di-boson production channels. However, dimension-8 effects in the EFT expansion are then generally expected to be significant as well, if the underlying UV interactions are not particularly strong. Therefore, inclusion of (dimension-6)² terms in principle implies losing model-independence within EFT [33]. On the other hand, there is certain sensitivity to the dimension-6 Wilson coefficients in the cross-sections and the reported limits are, therefore, to be understood as conservative constraints.

There are many LHC analyses, a partial list includes Refs. [11, 12, 34, 35]. Thus far, many $VV \rightarrow VV$ processes have been discovered, but within errors agree with the SM. Interestingly, current experimental precision does not constrain the “weak coupling” regime, leaving plenty of space for new physics effects. It is particularly attractive since the uncertainties after LHC Run 2 are (by far) “statistics-dominated” [11].

The paper is organized as follows. In section 2, we present the relevant EFT-operators and motivate theoretically, by using analytical formulae from Appendix A, the more technical subsequent analysis. The core numerical analysis for VBS at (HL-)LHC is presented in section 3. We conclude with section 4.

2 Warming-up: $W^+W^+ \rightarrow W^+W^+$ scattering

As we mention in the introduction, although LHC experimental analyses of VBS are optimized for QGCs (dimension-8 operators), it is important, if not necessary, to examine the impact on TGCs (dimension-6 operators) on “golden” process $W^+W^+ \rightarrow W^+W^+$.⁶ After all, dimension-6 operators arise at leading order in EFT expansion. At tree level in SM EFT, as we prove explicitly, the process $W^+W^+ \rightarrow W^+W^+$ is gauge invariant, that is independent of the gauge fixing parameter, and hence its self-study is at least legitimate. In both SM and SM EFT at leading order there are seven Feynman diagrams shown in Fig. 2, mediated by a photon, a Z and a Higgs-boson in both t - and u -channels plus a contact diagram. Following closely the Warsaw basis notation [15], the Lagrangian (1.1) is affected at tree-level by 5 CP-Conserving and 3 CP-Violating, dimension-6, operators arranged in Table 1.

⁵Notice, however, the discussion in ref. [32]

⁶In section 3 we also examine the effect of “background” dimension-6 operators entering in other sub-processes.

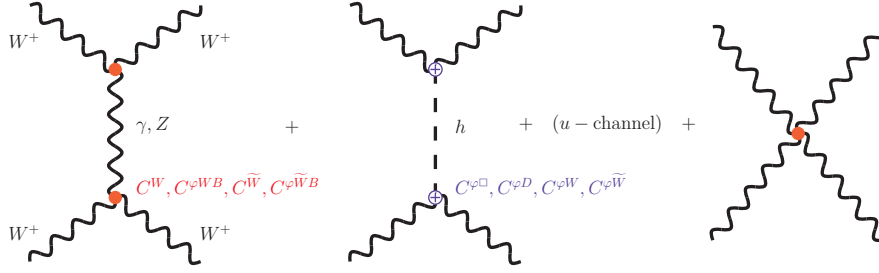


Figure 2: Tree level Feynman diagrams filling in the white blob of Fig. 1. Associated Wilson-coefficients to operators affecting each vertex are also shown.

	X^3	$\varphi^4 D^2$	$X^2 \varphi^2$
CPC	$Q_W = \epsilon^{IJK} W_\mu^{\nu I} W_\nu^{\rho J} W_\rho^{\mu K}$	$Q_{\varphi\Box} = (\varphi^\dagger \varphi) \Box (\varphi^\dagger \varphi)$ $Q_{\varphi D} = (\varphi^\dagger D^\mu \varphi)^* (\varphi^\dagger D_\mu \varphi)$	$Q_{\varphi W} = \varphi^\dagger \varphi W_{\mu\nu}^I W^{\mu\nu I}$ $Q_{\varphi WB} = \varphi^\dagger \tau^I \varphi W_{\mu\nu}^I B^{\mu\nu}$
CPV	$Q_{\widetilde{W}} = \epsilon^{IJK} \widetilde{W}_\mu^{\nu I} W_\nu^{\rho J} W_\rho^{\mu K}$		$Q_{\varphi \widetilde{W}} = \varphi^\dagger \varphi \widetilde{W}_{\mu\nu}^I W^{\mu\nu I}$ $Q_{\varphi \widetilde{WB}} = \varphi^\dagger \tau^I \varphi \widetilde{W}_{\mu\nu}^I W^{\mu\nu I}$

Table 1: Dimension-6 operators, in the Warsaw basis, modifying the process $W^+W^+ \rightarrow W^+W^+$.

The leading high energy helicity amplitudes are given in Appendix A. We work in the Warsaw basis and use the Feynman rules in R_ξ -gauges from ref. [36]. The operators $Q_{\varphi WB}$, and $Q_{\varphi \widetilde{WB}}$ disappear from leading- s helicity amplitudes in $WW \rightarrow WW$ processes. This is easily seen by just looking at the SM EFT Feynman Rules and use the Goldstone boson equivalence theorem [37–43], where for these operators and specifically to $WW \rightarrow WW$ channel, there are no associated contact four-point interactions involving Goldstone bosons nor exist a contact interaction with four W 's proportional to $C^{\varphi WB}$ or $C^{\varphi \widetilde{WB}}$. One may think that there may be contributions from gluing the 3-point vector boson vertices shown in Fig. 2 where these insertions exist, but it can be proved explicitly that any s -enhanced amplitude cancels out when consistently expanding the Z -mass, also affected by $C_{\varphi WB}$. Another feature of importance is the appearance of the t -channel enhancement $(1 - \cos^2 \theta)$, where θ is the scattering angle, in the denominator of leading SM amplitudes, see, for example \mathcal{M}_{++++} in (A.11). This is in contrast to the fact that none of SM EFT amplitudes has such a t -channel enhanced factor that is accompanied by a growth of energy, see eqs. (A.17)-(A.25).

Furthermore, in Appendix A.1 we also arrange analytical expressions for the helicity cross sections following the notation where “ T ” stands for transverse helicities ± 1 and “ L ” for longitudinal gauge bosons with helicity-0. In the SM, the dominant polarized cross-sections come into the following rates:

$$\sigma_{TTTT} : \sigma_{LLLL} : \sigma_{LTLT} : \sigma_{TLTL} : \sigma_{TLLT} : \sigma_{LTTL} \approx 1 : \frac{1}{8.5} : \frac{1}{8.0} : \frac{1}{8.0} : \frac{1}{8.0} : \frac{1}{8.0}. \quad (2.1)$$

As we already mentioned, in the SM all polarized cross sections are enhanced by the t -channel factor but, particularly for the $TTTT$ -mode there is an accidentally enhanced factor of 8 w.r.t. the other modes as can easily be seen from eqs. (A.26)-(A.28).

In SM EFT there are interference effects between the SM and dimension-6 operators only in the $LLLL$ -mode (or “0000” mode). CP-violating contributions enter in the mixed and pure transverse

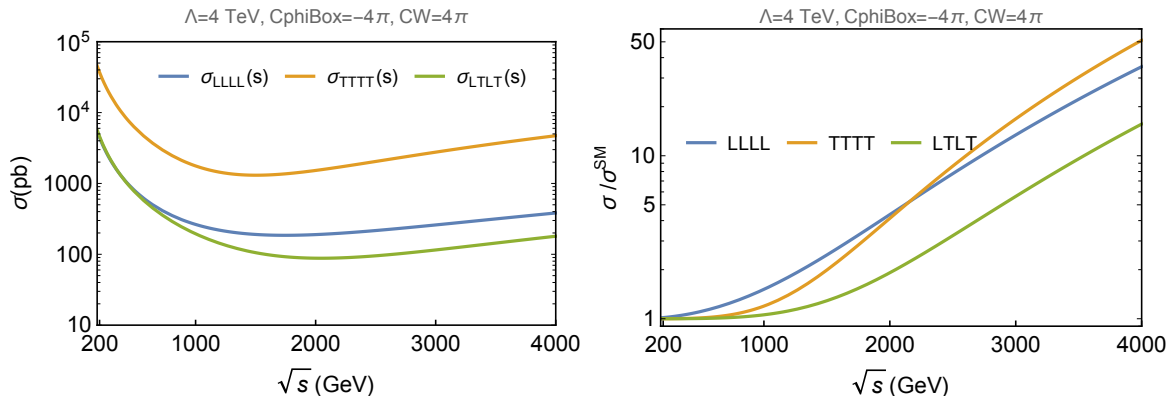


Figure 3: *Left:* Polarized cross sections for the three mode cross sections, eqs. (A.26)-(A.28), as a function of the c.m energy \sqrt{s} . We have chosen as input values the coefficients shown at the top of the figures and $\theta_{cut} = \pi/18$. *Right:* Similarly for the ratios of the polarized cross sections w.r.t the SM result.

channels, similar to their CP-conserving counterparts. The cross sections have the symbolic form $\sigma \sim \text{SM}^2 + \text{SM} \times \text{dim6} + \text{dim6}^2$. Following this pattern we obtain (\bar{g}^2 is the $SU(2)_L$ gauge coupling):

$$\sigma_{TTTT}(s) \approx \frac{\bar{g}^4}{s} \left[\frac{A_T}{1-c^2} + B_T \cdot 0 + \Gamma_T \bar{g}^2 \left(\frac{|C^W|}{\bar{g}^2} \right)^2 \left(\frac{s}{\Lambda^2} \right)^2 + \dots \right], \quad (2.2)$$

$$\sigma_{LLLL}(s) \approx \frac{\bar{g}^4}{s} \left[\frac{A_L}{1-c^2} + B_L \left(\frac{C^{\varphi\Box}}{\bar{g}^2} \right) \left(\frac{s}{\Lambda^2} \right) + \Gamma_L \left(\frac{C^{\varphi\Box}}{\bar{g}^2} \right)^2 \left(\frac{s}{\Lambda^2} \right)^2 + \dots \right], \quad (2.3)$$

where A_i, B_i, Γ_i ($i = T, L$) are dimensionless coefficients read from eqs. (A.26) and (A.27) that depend upon the cutting angle $c \equiv \cos(\theta_{cut})$ and ratios of vector boson and Higgs masses, and “...” are corrections from higher than six dimensional operators. The corresponding expression for σ_{LTLT} and related cross-sections are similar in form with (2.2). In order to justify clearly our points, we focus only on C^W and $C^{\varphi\Box}$ contributions in eqs. (2.2)-(2.3). Full analytical expressions are given in Appendix A, eqs. (A.26)-(A.28).

In a *weakly coupled* UV-theory with perturbative decoupling, dimensional analysis [44] results in $C^W \approx g^3/(4\pi)^2, C^{\varphi\Box} \approx g^2$. These effects could be important only if $A_L \approx (1-c^2)B_L(s/\Lambda^2)$ which is never the case for $c \approx 1$ and $s < \Lambda^2$, which suggests weak sensitivity to small coupling regime in the W^+W^+ process. This result, however, does strongly depend on the cutting-angle θ_{cut} . For example, in differential cross-section distributions for the $LLLL$ -mode, there are zeros for different values of SM EFT $C^{\varphi\Box}$ and/or $C^{\varphi D}$ input values! This case study is however statistics limited at LHC mainly because the SM dominant $TTTT$ -mode will not be affected, but may be important for future HL-LHC studies.

In a *strongly coupled* UV-theory or in a UV-theory with *composite gauge bosons* the loop-suppression of C^W may not be dictated by gauge invariance. Naive dimensional analysis [45] in such an extreme case may result in SM EFT coefficients as big as $C^W \approx 4\pi$ and $C^{\varphi\Box} \approx (4\pi)^2$. What is most important here is the fact that the prefactors in eq. (2.2), $\Gamma_T = 36\sqrt{2}/\pi$ and $A_T = 64/\pi$ are quite big and of the same order of magnitude. This guarantees large cross-sections and visible effects in SM EFT. For example, if $C^W = C^{\varphi\Box} \gg 1$ then the $TTTT$ -mode is again bigger than $LLLL$ -mode cross section by a factor of $g^2\Gamma_T/\Gamma_L = 144\sqrt{2}(G_F m_W^2) \simeq 15$. In this case, only contributions with dim6^2 in eqs. (2.2)-(2.3) are dominant, an approximation which is independent

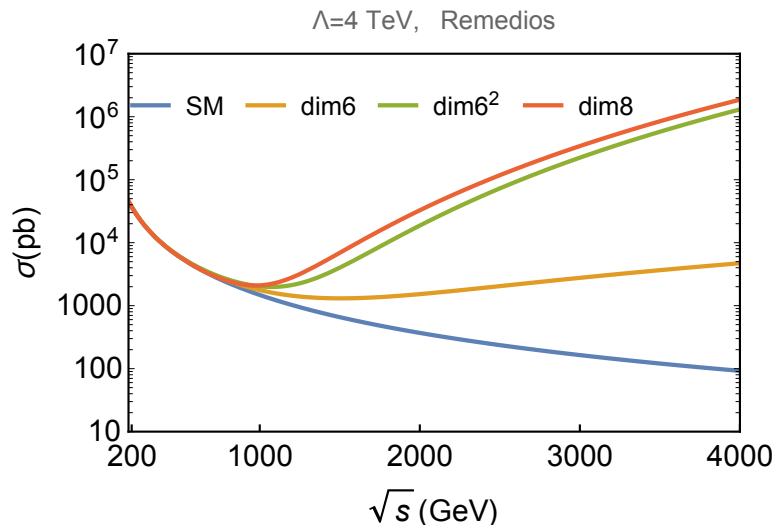


Figure 4: Effects of (dimension-6)² and dimension-8 operators contributions for $C^W = g_*$, $C^{t0,t1,t2,t10} = g_*^2$, with $g_* = 4\pi$ in the so called Remedios model for W^+W^+ elastic scattering. The curves show the transversely polarized cross section, σ_{TTTT} , starting from the SM (lower curve), ending at the full SM+dim6+dim6²+dim8 (upper curve) helicity amplitudes. In Remedios the cross-section cannot be smaller than the dim6-curve (orange curve).

from the cutting-angle θ_{cut} .

We demonstrate these effects in Fig. 3. We have chosen $\Lambda = 4$ TeV, and, two non-zero Wilson coefficients: $C^W = 4\pi$ which affects only the $TTTT$ - and $LTLT$ -modes and $C^{\varphi\Box} = -4\pi$ which affects only the $LLLL$ -mode.⁷ The set of input values, although indicative, are consistent with the bounds from diboson production and electroweak fits [28] (see below) when marginalized over other coefficients. Obviously the appearance of factors $(s/\Lambda^2)^n$, $n = 1, 2$ in eqs. (A.26)-(A.28) turns the cross sections to rising. As explained, the dominant mode is the σ_{TTTT} , i.e., the effect of C^W seems the most promising. The step rising of the $LLLL$ -cross section for low \sqrt{s} is due to the interference of SM and new physics arising from dimension-6 operators. From the right panel of Fig. 3 it is obvious that the $TTTT$ and $LLLL$ cross sections are enhanced by a factor of ~ 10 much before the EFT validity upper bound⁸, $s \approx \Lambda^2$, which is encouraging to make us proceed to a more realistic VBS analysis at the LHC. We do this in the next section.

Furthermore, in the case of transverse gauge boson scattering, we considered the effect of dimension-8 operators. It is well known [46, 47] that dimension-8 operators may dominate (up-to cancellations between coefficients induced by the UV-theory) the VBS cross-sections at energies

$$\frac{s}{\Lambda^2} \gg \frac{\bar{g}}{g_*}. \quad (2.4)$$

Here we consider the case of strongly coupled (or composite) transverse polarizations of W 's, in the so called Remedios models of ref. [46]. In these models, $C^W \sim g_*$ and $C^{t0,t1,t2,t10} \sim g_*^2$ with the later being the Wilson coefficients of dimension-8 operators defined in Appendix A.2. There, we have calculated all dominant helicity amplitudes with leading- s and s^2 behaviour. All but one independent helicity amplitudes are masked by the t -channel photon and Z -boson exchange

⁷The minus sign in $C^{\varphi\Box}$ results in constructive interference.

⁸Tree-level unitarity bounds are discussed in detail the in next section.

from the SM. The exception is the helicity violating amplitude \mathcal{M}_{++--} (or \mathcal{M}_{---+}). When the coupling g_* of the integrated UV-theory is strong, i.e. much larger than the $SU(2)$ -gauge coupling \bar{g} , these amplitudes give a large and positive contribution to the cross section. We therefore conclude, that the inclusion of only the dimension-6 operator C^W is a *robust conservative limit* to W^+W^+ VBS. Notice also that (dimension-6)² contributions in the amplitude come with opposite sign to the dimension-8 contributions when positivity constraints [48–50] are taken into account, which improves the EFT convergence.⁹ The situation is clearly explained in Fig. 4.

It is remarkable that in the case of Remedios-like scenarios the estimate on Wilson coefficients, based on power counting as given in ref. [46], does not allow for fulfilment of positivity bounds. This suggests that positivity constraints, eqs. (6.7)-(6.12) of ref. [49], constitute a significant limitation to models with composite dynamics of transverse electroweak modes. Notice however that these conditions can still be satisfied if e.g. departures from the power counting estimate is present in strongly coupled regime such as $C^{t0} = C^{t1} = C^{t10} = |C^W|^2 = g_*^2$ and $C^{t2} \geq 5g_*^2$.

3 The realistic study: $pp \rightarrow jjW^+W^+$ at the LHC

In this section we describe the steps of our analysis and present numerical results relying on Monte Carlo simulations. The reaction in question is $pp \rightarrow jjW^+W^+ \rightarrow jjll'\nu_l\nu_{l'}$, where $l = e^+, \mu^+$. The main goal is to estimate possible effects in same-sign WW scattering in the HL-LHC setup via the EFT approach. We analyse in an uncorrelated way one operator at a time while setting all the remaining Wilson coefficients to zero. Strictly speaking the above choice implicitly assumes certain subset of BSM scenarios where it is valid. Indeed, it constitutes a realistic assumption, e.g. (a) in the case of certain universal models with only bosonic weakly coupled BSM sector [52, 53] (given the current experimental constraints on EFT coefficients), (b) scenarios in which transversal modes of vector bosons have composite origin [46, 53]. Nevertheless, the only non-trivial aspect the above simplification misses, is interference terms between different operators. Given the fact that different operators interfere only if they modify the same helicity amplitudes [54], it is significantly limited in our set-up by just looking at eqs (A.17)-(A.25) of the Appendix A.

Below we focus on largest possible deviations using as our “benchmarks” the experimentally allowed boundary values for each f_i in eq. (1.1). We take as the source both the individual-operator-at-a-time limits and those from the global fit for physics scenarios complementarity. In the latter case, correlations between different operators are in principle important. We shall comment on the validity of our one-operator-at-a-time analysis below. Alike, we shall also discuss the effects of background EFT operators.

3.1 Perturbative Unitarity Bounds and Unitarization issues

The EFT operators in Table 1 induce $WW \rightarrow WW$ amplitude growth [see eqs (A.17)-(A.25)] which ultimately leads to violation of probability conservation at some energy scale $\sqrt{s^U}$, a certain WW -pair invariant mass, the latter being a function of f_i . In principle it may happen that $\sqrt{s^U}$ is within the accessible range of WW -mass and we found that, in fact, it is the case sometimes. Since predictions of the EFT amplitudes are ill-defined above $\sqrt{s^U}$, the issue has to be addressed in some way in the analysis. In this work we applied additional weights to events above $M_{WW} = \sqrt{s^U}$ in the

⁹See [51] for an interesting example in which the growth with energy, although substantial, does not lead to limitations due to pure EFT convergence. Cases studied are operators that contribute to neutral aTGCs. Such operators start at dimension-8 in SM EFT. Interestingly the identified observables at e^+e^- -colliders feature (dimension-8)² terms suppression, leading to “genuine” dimension-8 analysis.

original non-regularized samples generated with Monte Carlo. The weights are in general operator-dependent. The applied procedure is supposed to ensure that the total WW -scattering BSM cross sections after regularization behave like $1/s$ for $M_{WW} > \sqrt{s^U}$, and so it approximates the principle of constant amplitude, at least after some averaging over the individual helicity combinations [55]. Our choice of unitarization is often referred to in the literature as the (helicity-averaged) ‘‘Kink’’ method.¹⁰ We found the above mentioned weight to be equal to $(\sqrt{s^U}/M_{WW})^{3.5}$ for operator Q_W and $(\sqrt{s^U}/M_{WW})^{1.5}$ for $Q_{\varphi\Box}$ and $Q_{\varphi W}$.¹¹ We refer to such unitarized signal estimate as total BSM signal.

Technically, $\sqrt{s^U}$ is determined by using the perturbative (tree-level) partial wave unitarity condition [57,58]. The statement on s^U from this condition is that for energies $s > s^U$ perturbativity of the EFT necessarily breaks down. In more detail, the unitarity limit has been determined by studying all helicity combinations for both W^+W^+ and W^+W^- elastic scattering amplitudes.¹² For each helicity amplitude, the first non-vanishing partial wave $\mathcal{T}^{(J)}$ (where always $J = 0, 1$ or 2) is identified and the unitarity bound is found. The scale where unitarity is violated, $\sqrt{s^U}$, is then identified as the lowest value among all such bounds. More explicitly, at tree-level the condition reads (for a detailed discussion see [59, 60])

$$\sqrt{N_{\lambda_a\lambda_b}N_{\lambda_1\lambda_2}} \left| \mathcal{T}_{\lambda_a\lambda_b;\lambda_1\lambda_2}^{(J)}(s) \right| \leq \frac{1}{2}, \quad (3.1)$$

where indices λ_a, λ_b (λ_1, λ_2) denote outgoing (incoming) helicities, whereas, $N_{xy} = 1/2$ for identical particles i.e. $x = y$, or otherwise $N_{xy} = 1$. Then the partial wave amplitudes, $\mathcal{T}_{\lambda_a\lambda_b;\lambda_1\lambda_2}^{(J)}(s)$, enter in the partial wave expansion as:

$$\mathcal{M}_{\lambda_a\lambda_b;\lambda_1\lambda_2} = 16\pi \sum_{J=0}^{\infty} (2J+1) \mathcal{T}_{\lambda_a\lambda_b;\lambda_1\lambda_2}^{(J)}(s) D_{\lambda_1-\lambda_2, \lambda_a-\lambda_b}^{(J)*}(\Omega_{\mathbf{p}(ab)}), \quad (3.2)$$

with $\Omega_{\mathbf{p}(ab)}$ is a solid angle in the direction $\mathbf{p}(ab) = \mathbf{p}_a + \mathbf{p}_b$, and $D_{m_J, \lambda}^{(J)}(\Omega_{\mathbf{p}})$ are the Wigner-functions satisfying the completeness relation

$$\int d\Omega_{\mathbf{p}} D_{m'_J, \lambda}^{(J')}(\Omega_{\mathbf{p}}) D_{m_J, \lambda}^{(J)*}(\Omega_{\mathbf{p}}) = \frac{4\pi}{2J+1} \delta_{J'J} \delta_{m'_J m_J}. \quad (3.3)$$

We analysed the terms that grow with energy ($\propto f_i$) in which case no Coulomb singularity occurs and correspondingly no phase-space regularization has to be applied (e.g. a cut of 1 deg in the forward and backward scattering regions). The results are cross-checked with VBFNLO 1.4.0 [61] for operators where direct applicability of the latter tool is possible in the context of Warsaw basis, obtaining good agreement in the unitarity limits. When applied, the unitarity bound scale, $\sqrt{s^U}$, will be denoted by vertical lines in M_{WW} distributions in figures below. Notice also that the unitarity bounds of VBS processes for dimension-6,8 operators were presented in refs. [62,63].

We would like to emphasise, that within the EFT approach one does not have knowledge what happens above s^U . It could be SM-like perturbative completion or the theory could be non-perturbative. In the former case one expects $\sim 1/s$ while in the latter $\sim (\log s)^2$, i.e. the saturation of Froissart bound [64] for the asymptotic behaviour of cross-sections. The Froissart bound has the advantage of working in non-perturbative sense and might be more appropriate in case of Q_W treatment – the latter is currently poorly constrained. Applying the Froissart bound to the tail

¹⁰See Ref. [56] for a review and comparisons between several unitarization schemes.

¹¹The different exponents follow from the fact that unitarity is first violated before the cross section gets dominated by its asymptotic terms.

¹²Both channels are governed by the same Wilson-coefficients.

would enhance the signal, although only slightly, as we argue below; hence our results are being somewhat onto the conservative side.

We verified that bulk of the SM EFT effect is within the EFT-valid region, i.e. originates from the region $s < s^U$. To this aim, we defined the ‘‘EFT-controlled’’ signal estimate [55] and compared it with the total BSM signal (the total BSM signal defined at the beginning of this section). The ‘‘EFT-controlled’’ signal estimate is calculated by replacing the generated high-mass tail $M_{WW} > \sqrt{s^U}$ with the one expected in the SM, while taking the EFT prediction for the region $M_{WW} < \sqrt{s^U}$. Hence, the ‘‘EFT-controlled’’ defines a signal originating uniquely from the operator within its (maximal) range of EFT validity. In turn, comparison between the total BSM signal estimate with the ‘‘EFT-controlled’’ signal allows for a verification of the significance of the tail region – the conclusions based on EFT are reliable only if bulk of the BSM signal is in the ‘‘EFT controlled’’ region [55]. In Sec. 3.4 we show that our results are approximately independent of how the contribution in the region above the unitarity bound, $s > s^U$, is estimated, i.e. this issue should be a secondary effect; quantitatively, we have checked that the total BSM signal and the ‘‘EFT-controlled’’ estimate are statistically consistent within 2σ for all the operators and Wilson coefficients studied in sec.3.4, with the exception of $f_W = 1 \text{ TeV}^{-2}$ (discussed further therein).

Although it is well known that non-unitarized results do not directly have a physics interpretation, they could be safely taken as overestimated upper bounds on any unitarized results. For this reason, agreement between non-unitarized results and the ‘‘EFT-controlled’’ estimate implies little dependence on unitarization details. We did the corresponding comparison in addition and we observe consistency within 2σ between non-unitarized results and the ‘‘EFT-controlled’’ results for all the cases (except $f_W = 1 \text{ TeV}^{-2}$). Therefore we choose to use the total BSM signal defined at the beginning of this section (popularly referred to as ‘‘Kink’’ method) to obtain our central results throughout this work.

Note also, that positivity bounds are not harmed by considering constant amplitudes for the asymptotic behaviour of cross-sections in our analysis.

3.2 Method and Kinematic variables

For the following analysis two samples of 6×10^5 events consistent with the VBS topology for the process $pp \rightarrow jj\mu^+\mu^+\nu\nu$ have been generated, each corresponding to a preselected arbitrary value of f_W or $f_{\varphi\Box}$ coefficient, in MadGraph5_aMC@NLO [65] v2.6.2 at LO at 14 TeV pp collision energy. Different f_i -values were obtained by applying weights to generated events, using the reweight command in MadGraph. The value $f_i = 0, \forall i$, represents the SM predictions for each study. Results for the remaining relevant operators, i.e. $Q_{\varphi D}, Q_{\varphi W}$, were obtained using the re-weight command with $Q_{\varphi\Box}$ sample.¹³

The SmeftFR code [66] v2.01 (based on FeynRules [67]) was used to generate the UFO file [68] with an input parameter scheme $\{G_F, m_W, m_Z, m_h\}$, in SM EFT. Cross sections at the output of MadGraph are multiplied by a factor 4x to account for all the lepton combinations in the final state. Hadronization is done with Pythia v8.2 [69, 70], run within MadGraph. Reconstruction level is generated via the MadAnalysis5 [71] v1.6.33 package (available within MadGraph). The FastJet [72] v3.3.0 package is used with the jet clustering anti-kT algorithm with radius=0.35 and ptmin=20. Finally, the detector efficiencies are set to 100%.

The SM process $pp \rightarrow jj\ell^+\ell^+\nu\nu$ is treated as the irreducible background, while the ‘‘signal’’ is defined as the enhancement of the event yield relative to the SM prediction in the presence of a given operator Q_i . None of the reducible backgrounds are simulated. The reason is that reducible backgrounds, as we learn from e.g. Fig. 3 of a recent study [11], roughly doubles the

¹³Samples for Q_W were generated separately due to large reported uncertainties when reweighting from $Q_{\varphi\Box}$.

total statistics overall in the VBS fiducial region and is mostly concentrated at low mass (both dilepton and dijet). Since VBS-related operators modify mainly the opposite end of the spectrum, reducible backgrounds probably will not be crucial to have an estimate of the possible effects. Yet another aspect is that additional operators might also modify the reducible backgrounds in some unforeseen ways. But such potential effects will need to be determined experimentally from other studies, in which those processes are not backgrounds but signals. We do not address this issue in our paper.

Following ref. [55], the event selection criteria consist of requiring at least two reconstructed jets and exactly two leptons (muons or electrons) satisfying the following conditions: $M_{jj} > 500$ GeV, $\Delta\eta_{jj} > 2.5$, $p_T^j > 30$ GeV, $|\eta_j| < 5$, $p_T^\ell > 25$ GeV and $|\eta_\ell| < 2.5$, being $\eta_{j,\ell}$ the pseudorapidity of jets j or leptons ℓ , respectively. The total BSM signal significances are computed as the square root of a χ^2 resulting from a bin-by-bin comparison of the event yields in the binned distributions of different kinematic observables. Moreover, event distributions are always normalized to HL-LHC luminosity, i.e. 3000 fb^{-1} .

For each benchmark value of $f_{i=W,\varphi\Box,\varphi D,\varphi W}$, the signal significance is assessed by studying the distributions of a large number of kinematic variables. These are:

$$\begin{aligned}
& m^{jjll}, m^{ll}, m^{jj}, p_T^{j1}, p_T^{j2}, p_T^{l1}, p_T^{l2}, \\
& \eta^{j1}, \eta^{j2}, \eta^{l1}, \eta^{l2}, d\eta^j, d\phi^j, d\phi^l, \\
& R_{p_T} \equiv p_T^{l1} p_T^{l2} / (p_T^{j1} p_T^{j2}), \\
& M_{o1} \equiv \sqrt{(|\vec{p}_T^{l1}| + |\vec{p}_T^{l2}| + |\vec{p}_T^{miss}|)^2 - (\vec{p}_T^{l1} + \vec{p}_T^{l2} + \vec{p}_T^{miss})^2}, \\
& M_{1T}^2 \equiv \left(\sqrt{(m^{ll})^2 + (\vec{p}^{l1})^2 + (\vec{p}^{l2})^2} + |\vec{p}_T^{miss}| \right)^2 - (\vec{p}^{l1} + \vec{p}^{l2} + \vec{p}_T^{miss})^2,
\end{aligned} \tag{3.4}$$

where $l1(2) \equiv$ (sub) leading lepton; $j1(2) \equiv$ (sub) leading jet; m invariant mass; $p_T^{(miss)} \equiv$ (missing) transverse momentum; $\eta \equiv$ pseudo-rapidity, $\phi \equiv$ azimuthal angle. Some of these variables are well known to be VBS-blind, but in the context of ‘‘background operator’’ they may still be useful. We found both angular variables, η s and ϕ s, as well as p_T s involving jet(s), to be at most sub-leading in sensitivity. Moreover, all p_T s, m s and M s were found to be at most sub-leading in sensitivity in case of $Q_{\varphi\Box}$ and $Q_{\varphi D}$. The most sensitive variables were found to be: p_T^{l1} for Q_W ; M_{o1} for $Q_{\varphi W}$; and R_{p_T} for $Q_{\varphi\Box}$, $Q_{\varphi D}$.

We considered one-dimensional distributions of single variable. Each distribution is divided into 10 bins, arranged so that the Standard Model prediction in each bin is never lower than 2 events. Overflows were always included in the respective highest bins. Presented results and conclusions are always based upon the most sensitive variables, which is, in general, an operator dependent outcome.

The total BSM signal significance expressed in standard deviations (σ) is defined as the square root of a χ^2 resulting from comparing the bin-by-bin event yields:

$$\chi^2 = \sum_i (N_i^{BSM} - N_i^{SM})^2 / N_i^{SM}. \tag{3.5}$$

$\psi^2\varphi^3$ [29]	σ	$\psi^2 X\varphi$ [29]	σ
$f_{u\varphi}$ $[-120., -36.] \times y_u$	0.027	f_{uG} $[+5, +18.] \times y_u$	5.5×10^{-3}
$f_{d\varphi}$ $[+3., +7.9] \times y_d$	0.		
$\psi^2\varphi^2 D$ [28]	σ	$(\bar{L}L)(\bar{L}L)$ [30,31]	σ
$f_{\varphi q}^{(1)}$ $[-0.23, +0.12]$	0.46	$f_{qq}^{(1)}$ $[-0.028, +0.057]$	1.1
$f_{\varphi q}^{(3)}$ $[-0.18, +0.17]$	5.7		
$f_{\varphi u}$ $[-0.79, +0.54]$	0.		
$f_{\varphi d}$ $[-0.81, +0.13]$	0.		
$(\bar{R}R)(\bar{R}R)$ [30]	σ	$(\bar{L}L)(\bar{R}R)$ [30]	σ
f_{uu} $[-0.1, +0.23]$	0.	$f_{qu}^{(1)}$ $[-0.35, +0.35]$	0.
f_{dd} $[-0.31, +0.44]$	0.	$f_{qu}^{(8)}$ $[-0.5, +1.]$	0.
$f_{ud}^{(1)}$ $[-0.44, +0.44]$	0.	$f_{qd}^{(1)}$ $[-0.59, +0.59]$	0.
$f_{ud}^{(8)}$ $[-0.59, +1.56]$	0.	$f_{qd}^{(8)}$ $[-1., +1.56]$	0.

Table 2: *Compilation of all the experimental limits coming from global fits on dimension-6 background operators used in this work, in TeV^{-2} units, and maximal effect in standard deviations (σ) in the W^+W^+ scattering process from each operator separately. Flavor assumptions are implicit and follow the references quoted. In particular, “ $\times y$ ” corresponds to the Minimal Flavor Violation assumption.*

3.3 Background Operators analysis

Before moving to the analysis of operators in Table 1 that modify the $WW \rightarrow WW$ reaction (VBS operators), we comment on the role of the dimension-6 interactions that, although do not affect the sub-process $WW \rightarrow WW$ directly, may contribute at parton level to $pp \rightarrow jjll'\nu_l\nu_l'$ (background operators). This is particularly relevant for consistency of the discussion of potential effects of VBS operators when f_i is constrained by the global fit, but also for a more complete description in general. We examined possible contributions (after the VBS cuts are applied) operator-by-operator, based on the bounds reported in [28, 29] (non-4-fermion operators, the global more permissive constraints are implicitly understood below) and [30, 31] (4-fermion operators) (with consistently applied flavor assumptions). The so-called “dipole” operators, i.e. $Q_{uW}, Q_{uB}, Q_{dG}, Q_{dW}, Q_{dB}$, are not present in the quoted references. They are however commonly claimed to be strongly constrained [29, 73]. We checked that among these, only Q_{uW}, Q_{dW}, Q_{dG} would lead to noticeable effects for a representative $f_i = 1 \text{ TeV}^{-2}$. Importantly however, they also lead to commonly distinctive kinematic features compared to VBS operators, and hence they are in principle easy to be separated as part of “background” effects (discussed in detail below). We have limited our examination to non-leptonic operators, because leptonic operators would contribute only at loop-level to the process $pp \rightarrow jjWW$, and it is known that the on-shell projection of the outgoing W 's can be defined in a gauge invariant way and constitute a fine ($\lesssim 5\%$ error) approximation [74, 75]. Moreover, in this work we do not consider CP- or B-violating operators. Out of the remaining, coefficients accompanied the operator Q_G are known to be constrained at $O(0.01) \text{ TeV}^{-2}$ via multi-jet channels [76], whereas, Q_φ does not contribute to the tree-level amplitude. We

also omit $Q_{\varphi G}$ as it is constrained by gluon fusion to Higgs-boson at loop-level [77]. In addition to this, we found no sensitivity to the 4-fermion operators in the “ $(\bar{L}R)(\bar{R}L)$ ” and “ $(\bar{L}R)(\bar{L}R)$ ” classes even for generic BSM coupling in the strong interaction regime. The experimental bounds on the remaining background operators are compiled in Table 2. One can see that strong suppression is hidden in the Yukawa factors for the $Q_{u\varphi}, Q_{d\varphi}, Q_{uG}$ interactions (Minimal Flavor Violation hypothesis is assumed throughout the analysis). Since the light quarks play (by far) the leading role in our reaction, the Wilson coefficients are effectively of, at least, 1-loop order in this case.

As far as non-4-fermion operators are concerned, we found that the current limits on all background dimension-6 operators yield cross-sections consistent with the SM prediction, with the exception of

$$Q_{\varphi q}^{(3)} = (\varphi^\dagger i \overleftrightarrow{D}_\mu^I \varphi) (\bar{q}_T^I \gamma^\mu q), \quad (3.6)$$

that yielded systematic discrepancy of around $\sim 5\%$. Detailed analysis revealed that this operator gives a up to $\approx 5.5\sigma$ potential discrepancy with SM at the HL-LHC. The distributions in M_{WW} and p_T^{j1} are shown in Fig. 6 for $f_{\varphi q}^{(3)} = +0.17$ (the negative boundary value $f_{\varphi q}^{(3)} = -0.18$ is very similar).

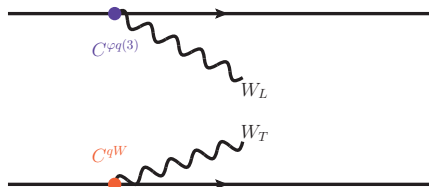


Figure 5: Examples of background operators indicated by the associated Wilson-coefficients.

One can observe that this background operator [see Fig. 5] has distinct dynamics compared to the VBS operators (presented subsequently). In particular, the contributions to χ^2 are uniformly distributed among all the bins (p_T^{j1}) and a similar feature holds for the M_{WW} distribution. That is expected, because this background operator has nothing to do with WW -mass, but as shown in Fig. 5 it mainly contributes to the hard scattering for longitudinal W -bosons, so the energy dependence measured in WW -processes should be different.

It shows that even when the background operator effect is large, it can be easily identified and disentangled by studying kinematic distributions – if one gets more than 5σ between $Q_{\varphi q}^{(3)}$ and the SM, then one is likely also to get a 5σ difference between the predicted shapes for $Q_{\varphi q}^{(3)}$ and any VBS operator. More quantitatively, we found e.g. that p_T^{j1} is the most sensitive variable in the case of $Q_{\varphi q}^{(3)}$ ¹⁴, while it is by far sub-leading in sensitivity for the VBS operators. Moreover, the weak sensitivity of jet- p_T s also holds for the leading dimension-8 operators [78] usually considered as the leading effects in phenomenological/experimental analyses for VBS processes so far. On the other hand, the highest sensitivity to p_T^{j1} also holds for the relevant dipole operators, as well as for the operator $Q_{\varphi ud}$, which is not studied in the “bounds” literature either; this constitutes the distinctive dynamics mentioned above for the dipole operators.

Concerning the potential effects in 4-fermion dimension-6 operators, we checked that the limits reported in [30] were already sufficient to claim negligible effects these operators might at most generate. The exception was the left currents operator $Q_{qq}^{(1)}$ for which the search in the more up-to-date ref. [31] was used to derive the factor by which the limits reported in [30] improve. We found the factor to be conservatively estimated by $\sim 3x$, and using the improved constraints concluded

¹⁴Notice, it involves a contact interaction between two quarks and two vectors, so it contributes to a hard scattering of qW .

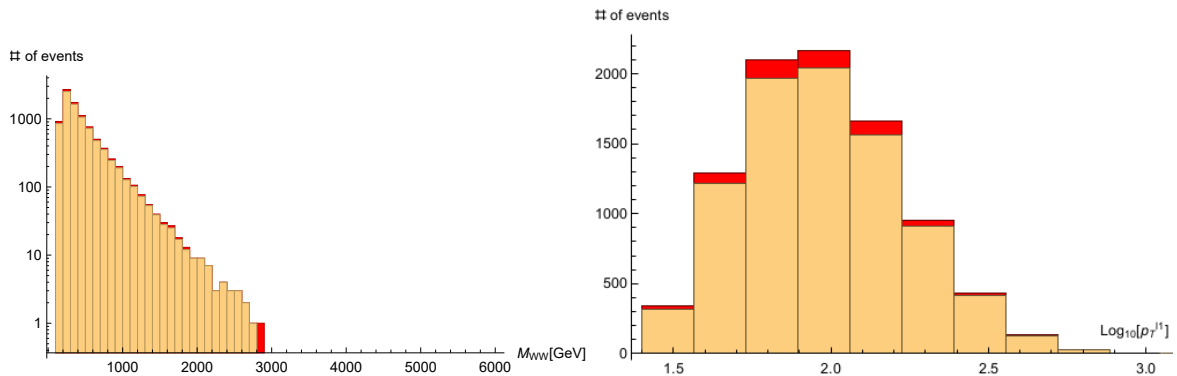


Figure 6: The distributions in WW system invariant mass M_{WW} (left) and the most sensitive observable (here p_T^{l1}) for $f_{\varphi q}^{(3)} = +0.17$ compared to the SM case. The BSM signal estimate is in red and the SM in yellow.

that the operator might generate only negligible effects. Note that the other non-leptonic operator in the $(LL)(LL)$ category, $Q_{qq}^{(3)}$, is identical to $Q_{qq}^{(1)}$ assuming flavor-diagonal Wilson coefficients.

3.4 Main operators analysis

From the previous subsection, we conclude that in practice it suffices to parametrize potential NP effects from Wilson coefficients associated with the main dimension-6 operators listed in Table 1. i.e. the operators that modify the $WW \rightarrow WW$ sub-process. By saying this we exclude from our discussion CP-Violating operators, $Q_{\widetilde{W}}$ and $Q_{\varphi\widetilde{W}}$ ¹⁵ for two reasons: first, because their contribution in the cross section $WW \rightarrow WW$ is no different than the CP-Conserving Q_W and $Q_{\varphi W}$, and second, these operators are (usually) much more constrained than their CP-Conserving cousins. Therefore, we focus on the CPC operators arranged in Table 1 for the numerical simulations to follow.

We begin by examining the possible effects at the HL-LHC assuming the bounds on EFT coefficients come from the individual-operator-at-a-time analysis, based on the recent [28]; we quote the relevant constraints indicated as “individual” in Table 3. The only f_i bounded by as

	f_W	$f_{\varphi\Box}$	$f_{\varphi D}$	$f_{\varphi W}$
“individual”	[-0.15,+0.36]	[-0.44,+0.52]	[-0.025,+0.0015]	[-0.014,+0.0068]
“global”	[-1.3,+1.1]	[-3.4,+2.4]	[-2.7,+1.2]	[-0.14,+1.6]

Table 3: Experimental constraints on the subset of operators modifying the process $W^+W^+ \rightarrow W^+W^+$: based on the individual-operator-at-a-time or global marginalized fit analyses; from [28].

large as $O(0.1)$ TeV^{-2} are $f_{\varphi\Box}$ and f_W , the remaining two $f_{\varphi D}$ and $f_{\varphi W}$ are bounded by $O(0.01)$ TeV^{-2} (or stronger, depending on the sign) and give null discrepancies with the SM. In fact, at the boundaries $f_{\varphi\Box} \approx \pm 0.5$ yields negligible effects as well. On the other hand, both boundaries on f_W allow for large effects. The distributions M_{WW} (left) and the total BSM signal in the most significant variable p_T^{l1} (right), are shown in Fig. 7 for $f_W = +0.36$ TeV^{-2} and in Fig. 8 for

¹⁵The operator $Q_{\varphi\widetilde{W}B}$ does not enter to the leading amplitudes, see formulae in Appendix A.1.

$f_W = -0.15 \text{ TeV}^{-2}$. Notice, that in the right plots the total BSM signal is drawn with red and

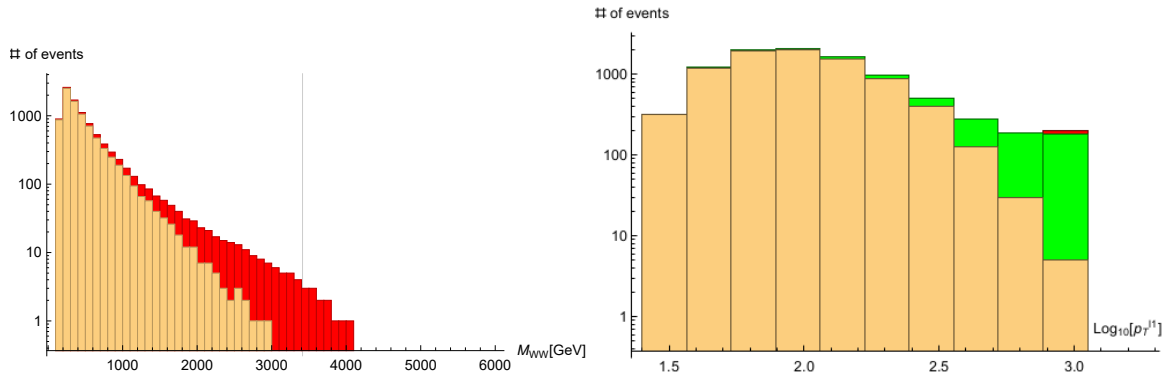


Figure 7: Distributions in WW pair invariant mass M_{WW} (left) and the most sensitive observable (right, here p_T^1), for $f_W = +0.36 \text{ TeV}^{-2}$ compared to the SM case. The total BSM signal estimate is in red and the SM in yellow. Notice, that in the right plot shown is the “EFT-controlled” signal estimate in green (almost identical to the red one); normalized to HL-LHC. The vertical line (left) denotes the scale above which the partial wave unitarity condition is violated (see Sec. 3.1).

the “EFT-controlled” signal with green, and that the red histogram is almost entirely covered by the green one, as anticipated in Sec. 3.1.

Next, we consider bounds on f_i from the global fit (indicated with “global” in Table 3), again based on recent literature [28]. One can observe that constraints here are considerably more relaxed than the “individual” ones allowing for f_i as large as $O(1.) \text{ TeV}^{-2}$. It is due to correlations between various Wilson coefficients that contribute to the same observables used to determine the bounds. Therefore such bounds could be understood as complementary and in principle saturated in UV models that normally allow for a plethora of dimension-6 coefficients without too large hierarchies in their magnitudes; e.g. one can construct such models exploiting the UV vs tree-level matching dictionary [52] with a large number of different heavy species. As no correlation matrix is provided in ref. [28], in what follows we examine the four VBS-operators in a simplified way, i.e. one-by-one, and describing qualitatively the effect of correlations below.

We take an estimate on correlations from ref. [29], which corresponds to similar physics assumptions. One can see that the correlations among the four relevant operators are mostly neg-

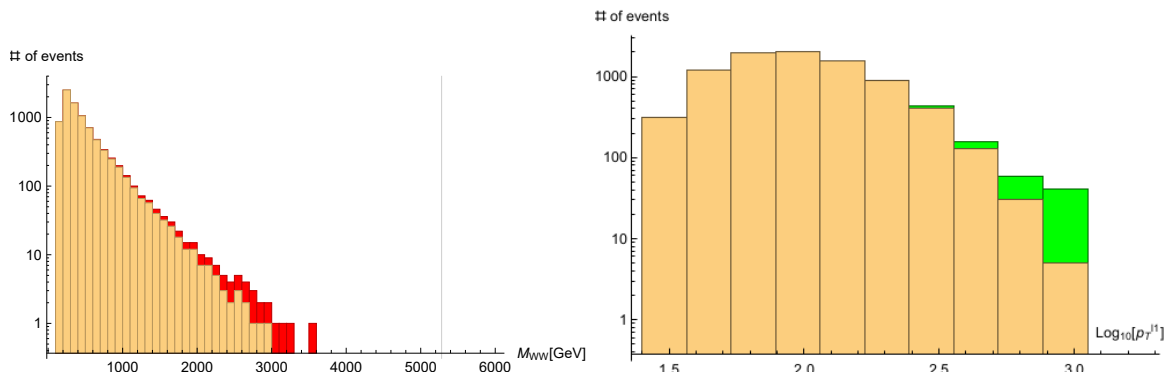


Figure 8: Like Fig. 7 for $f_W = -0.15 \text{ TeV}^{-2}$.

ligible. They are however somewhat mild between the following pairs: $(Q_{\varphi\Box}, Q_{\varphi W})$, $(Q_{\varphi\Box}, Q_W)$, $(Q_{\varphi D}, Q_W)$. Since, as we show in the Appendix, the operators in each pair modify distinct helicities of the $WW \rightarrow WW$ sub-process, the corresponding effects do not interfere. As a result, to account for correlations corresponds to adding together the effects presented in this work of each operator, with appropriate weights from the correlation matrix. The most sensitive variables in (3.4) for each operator feature increase of number of events in the higher (relevant) bins independently of the sign of f_i . Moreover, notice that the account for mild correlation with Q_W may affect the estimated effects because this operator is by far dominant in our analysis, and in this sense the results presented below for $Q_{\varphi\Box}$ and $Q_{\varphi D}$ should be regarded as conservative ones.

The distributions in M_{WW} together with the most sensitive variable, are shown in Figs. 9, 10, 11 and 12 for operators $Q_{\varphi D}$, $Q_{\varphi W}$, $Q_{\varphi\Box}$ and Q_W , respectively (for $f_{i=\varphi D, \varphi W, \varphi\Box}$ at the relevant, either positive or negative, boundary).

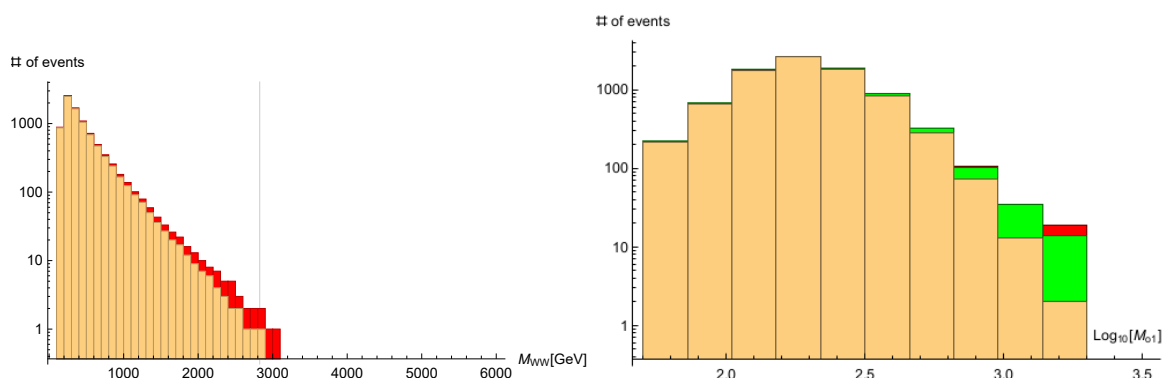


Figure 9: Like in Fig. 7 for $f_{\varphi W} = +1.6 \text{ TeV}^{-2}$.

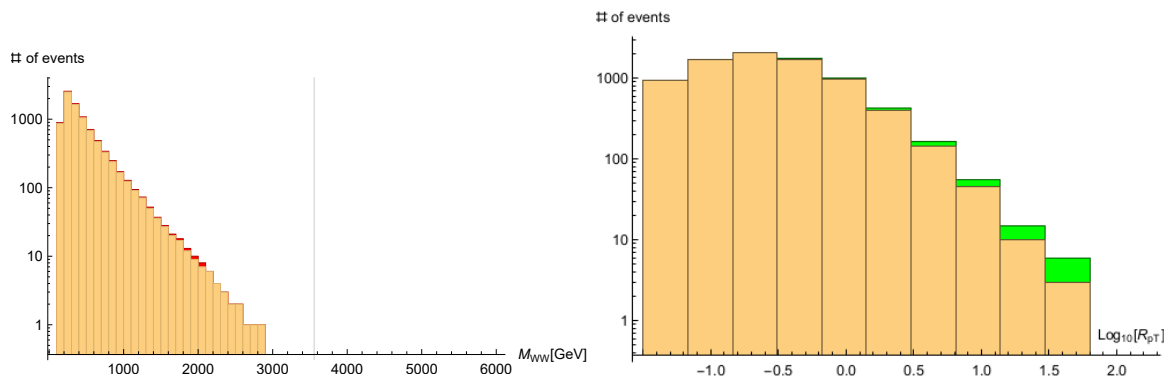


Figure 10: Like in Fig. 7 for $f_{\varphi D} = -2.7 \text{ TeV}^{-2}$.

As above, it is worth noticing that for all operators, the bulk of the SM EFT effect is within the EFT-valid region. In terms of standard deviations (σ), the maximal discrepancies for $Q_{\varphi D}$, $Q_{\varphi W}$, $Q_{\varphi\Box}$ at the HL-LHC allowed by current data read as 4.4, 15., 12. σ , respectively. Hence these operators cannot be, in general, simply neglected in studies for HL-LHC prospects of discovery potential via the EFT approach.

The possible effects from Q_W are, in accord with Sec. 2, exceptionally large – the obtained discrepancy at the HL-LHC is $O(100.)\sigma$. In this case the exact number of σ s may vary depending

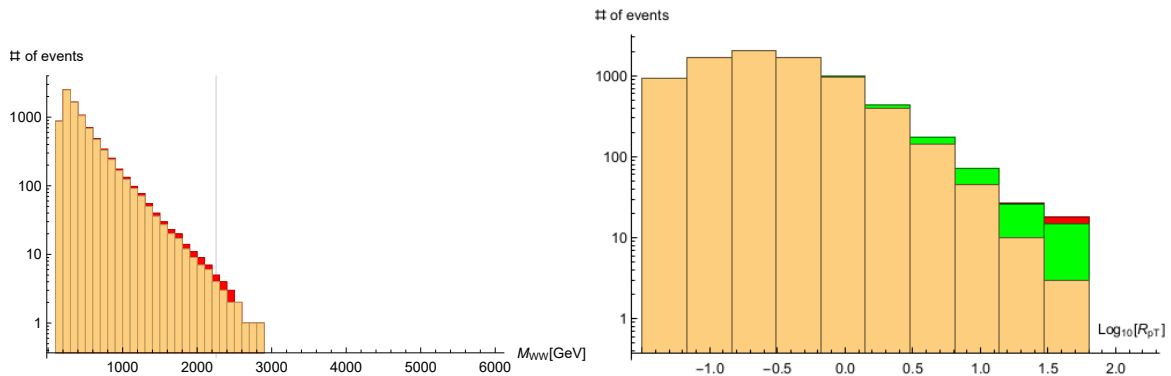


Figure 11: Like in Fig. 7 for $f_{\varphi\Box} = -3.4 \text{ TeV}^{-2}$.

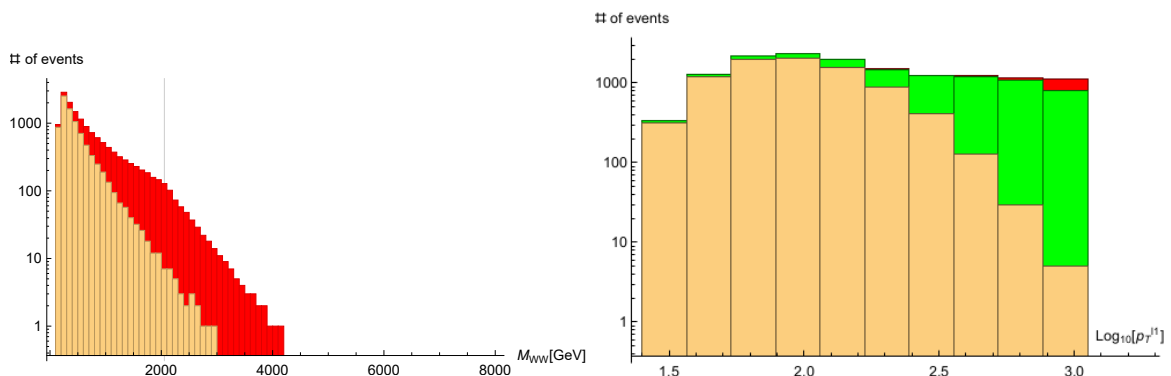


Figure 12: Like in Fig. 7 for $f_W = +1. \text{ TeV}^{-2}$.

on the chosen method of unitarization, as anticipated in Sec. 3.1. For the scope of this paper it is rather inessential, so we report only the order of magnitude. Clearly, signal significance can be huge, much above 5σ even in the “EFT-controlled” estimate, therefore not at all negligible in VBS data analyses in the HL-LHC perspective. Moreover, a simple rescaling to current luminosity, would imply large possible discrepancies already in the currently collected LHC dataset. Though counter-intuitive at first sight, it is partially a result of truncating the cross-section consistently at dimension-6, which, as already discussed in the introduction, leads to conservative bounds from di-boson production channel. Although the same-sign WW scattering studies illustrate the necessity for better theoretical understanding (and as a consequence improvement) in setting constraints based on di-boson production at LHC, it also shows (i) large potential in VBS processes to set constraints on the f_W coefficient or alternatively (ii), by comparison of the red and green histograms in the right plots in Fig. 7 and 12, large discovery potential which is quantifiable by (seizable) “EFT-triangle” [55]; interestingly, the EFT-triangles for dimension-8 interactions are very limited [54, 55], due to EFT-validity issues caused by necessarily large high- M_{WW} tails, which makes indirect searches in transversal WW scattering via dimension-6 even more attractive.

4 Epilogue

In this article, we performed a detailed study of SM EFT effects from dimension-6 operators in a VBS process with like-sign- W production proceeding to leptonic final states. We studied

all relevant dimension-6 operators at tree level which are responsible for NP in VBS including “background” operators responsible for NP in non-VBS parts of the full process $pp \rightarrow jj\ell\ell'\nu\nu'$. In addition, in our analysis we exploited all available constraints on SM EFT Wilson coefficients and also derived the relevant perturbative unitarity bounds. The latter are applied to obtain quantitative estimate on the role of high-energy tails that cannot be described within the EFT approach. We have presented useful analytical formulae which illustrate and support the robustness of our simulations’ results.

	\mathcal{O}_W	$\mathcal{O}_{\varphi\Box}$	$\mathcal{O}_{\varphi D}$	$\mathcal{O}_{\varphi W}$
$\sigma^{HL-LHC} \leq$	O(100.)	12.	4.4	15.

Table 4: Maximal effect estimates in standard deviations (σ) for the relevant dimension-6 interactions in same-sign WW scattering allowed within present constraints as reported in the global fit analysis of [28] all normalized to HL-LHC.

We found that the role of dimension-6 operators in modifying the $W^+W^+ \rightarrow W^+W^+$ process can *not* be neglected in full generality, particularly for perspective studies at the HL-LHC based on current constraints. This is particularly true when the constraints on dimension-6 operators are taken from the global fit type analyses. The potential effect based on current global fit limits is summed up in Table 4 for the relevant operators. It shows a particular sensitivity to strong dynamics for transverse W -polarization, effects of which can be conservatively estimated with dimension-6 truncated amplitudes. Plausibly, the background operators are already constrained strongly enough to claim they play no role in WW -scattering process even under the HL-LHC perspective, with the exception of $Q_{\varphi q}^{(3)}$ operator (and potentially $Q_{\varphi ud}$ and dipole operators). These VBS-polluting operators, however, feature very distinctive dynamics, and they can be separated by studying different kinematic distributions.

Acknowledgements

We would like to thank Janusz Rosiek for his help in handling input parameter schemes in SmeftFR code. AD would like to thank Lambros Trifyllis and Kristaq Suxho for cross-checking a number of helicity amplitudes. PK is supported by the Spanish MINECO project FPA2016-78220-C3-1- P (Fondos FEDER), A-FQM-211-UGR-18 (Junta de Andalucía, Fondos FEDER) and by National Science Centre, Poland, the PRELUDIUM project under contract 2018/29/N/ST2/01153. The research of MS has been partly supported by VBSCan (COST action CA16108). We acknowledge partial support from National Science Centre, Poland, grant DEC-2018/31/B/ST2/02283.

Appendix A Helicity Amplitudes and Cross-Sections

Probably the best way to write down the anatomy of a cross section, especially for vector boson scattering, is to calculate first the helicity amplitudes for the given process. Being definitive, lets assume the elastic scattering of W^+ -gauge bosons,

$$W^+(p_1, \lambda_1) + W^+(p_2, \lambda_2) \rightarrow W^+(p_3, \lambda_3) + W^+(p_4, \lambda_4) . \quad (\text{A.1})$$

We consider the scattering plane to be the xz plane with \vec{p}_1 in $+\hat{z}$ direction, with the outgoing particle-3 momentum p_{3x} in positive \hat{x} -direction. More specifically, the kinematics are given by

$$p_1 = (E, 0, 0, p), \quad (\text{A.2})$$

$$p_2 = (E, 0, 0, -p), \quad (\text{A.3})$$

$$p_3 = (E, p \sin \theta, 0, p \cos \theta), \quad (\text{A.4})$$

$$p_4 = (E, -p \sin \theta, 0, -p \cos \theta). \quad (\text{A.5})$$

The center-of-mass scattering angle θ is restricted in $\theta \in [0, \pi]$ interval. For process (A.1) we have 81 helicity amplitudes. However, not all of them are distinct because of $C-$, $P-$, and $T-$ transformations as well as rotational invariance of the S -matrix. For example, CPT and CP transformations read as

$$\text{CPT - symmetry : } \mathcal{M}_{\lambda_1, \lambda_2, \lambda_3, \lambda_4}(\theta) = \mathcal{M}_{-\lambda_3, -\lambda_4, -\lambda_1, -\lambda_2}(\theta), \quad (\text{A.6})$$

$$\text{CP - symmetry : } \mathcal{M}_{\lambda_1, \lambda_2, \lambda_3, \lambda_4}(\theta) = \mathcal{M}_{-\lambda_2, -\lambda_1, -\lambda_4, -\lambda_3}(-\theta), \quad (\text{A.7})$$

relate the amplitudes up-to a phase factor [50, 79].

For an elastic polarized cross section like $W^+(\lambda_1)W^+(\lambda_2) \rightarrow W^+(\lambda_3)W^+(\lambda_4)$ we have

$$\left(\frac{d\sigma}{d\Omega}\right)_{\lambda_1\lambda_2\lambda_3\lambda_4} = \frac{1}{64\pi^2 s} |\mathcal{M}_{\lambda_1\lambda_2\lambda_3\lambda_4}(s, \cos \theta)|^2, \quad (\text{A.8})$$

while for unpolarized ones we have to sum over final and initial helicities and average over initial helicities

$$\left(\frac{d\sigma}{d\Omega}\right)_{\text{unpolarized}} = \frac{1}{9} \sum_{\lambda_1, \lambda_2 = -1}^1 \sum_{\lambda_3, \lambda_4 = -1}^1 \left(\frac{d\sigma}{d\Omega}\right)_{\lambda_1\lambda_2\lambda_3\lambda_4}. \quad (\text{A.9})$$

The integrated cross-section is defined as

$$\sigma(s) = \int_0^{2\pi} d\varphi \int_{\theta_{cut}}^{\pi - \theta_{cut}} d\theta \sin \theta \frac{d\sigma}{d\Omega}, \quad (\text{A.10})$$

where θ_{cut} is an angular cut in scattering angle.

We append in A.1 the helicity amplitudes $\mathcal{M}_{\lambda_1\lambda_2\lambda_3\lambda_4}$ in SM EFT with dimension-6 operators by keeping the SM contributions to $O(1)$ and up to leading $O(s)$ -amplitudes associated with the operators appeared in Table 1. We also append in A.2 a relevant to our discussion, partial list of amplitudes for SM EFT dimension-8 operators at leading $O(s^2)$. In calculating the amplitudes, we follow the notation of ref. [36] for vertices while we use the `SmefTFR` [66] to output Feynman Rules as input to `FeynArts` [80] and `FormCalc` [81] for amplitude calculations. In case of longitudinal vector boson scattering we have checked our results analytically with the Goldstone boson equivalence theorem [37–43].

A.1 Helicity amplitudes for $W^+(\lambda_1)W^+(\lambda_2) \rightarrow W^+(\lambda_3)W^+(\lambda_4)$ in SM EFT

The SM leading $\mathcal{O}(1)$ contributions, where λ is the Higgs-self coupling and \bar{g} the SM EFT improved $SU(2)_L$ -gauge coupling, are:

$$\mathcal{M}_{\pm\pm\pm\pm} = -\frac{8\bar{g}^2}{1 - \cos^2\theta}, \quad (\text{A.11})$$

$$\mathcal{M}_{\pm\mp\mp\pm} = -2\bar{g}^2 \frac{(1 - \cos\theta)}{(1 + \cos\theta)}, \quad (\text{A.12})$$

$$\mathcal{M}_{\pm\mp\pm\mp} = -2\bar{g}^2 \frac{(1 + \cos\theta)}{(1 - \cos\theta)}, \quad (\text{A.13})$$

$$\mathcal{M}_{0\pm 0\pm} = \mathcal{M}_{\pm 0\pm 0} = -2\bar{g}^2 \left(\frac{1}{1 - \cos\theta} \right), \quad (\text{A.14})$$

$$\mathcal{M}_{\pm 0 0\pm} = \mathcal{M}_{0\pm\pm 0} = -2\bar{g}^2 \left(\frac{1}{1 + \cos\theta} \right), \quad (\text{A.15})$$

$$\mathcal{M}_{0000} = \frac{1}{2}(\bar{g}^2 + \bar{g}'^2) \left(1 - \frac{4}{\sin^2\theta} \right) - 2\lambda. \quad (\text{A.16})$$

The SM EFT leading- s contributions from CP-Conserving couplings associated to operators in the CPC row in Table 1 are:

$$\mathcal{M}_{\pm\mp\mp\mp} = \mathcal{M}_{\mp\pm\pm\pm} = \mathcal{M}_{\mp\mp\pm\pm} = \mathcal{M}_{\mp\pm\pm\pm} = -6\bar{g}C^W \frac{s}{\Lambda^2}, \quad (\text{A.17})$$

$$\mathcal{M}_{\pm\pm\mp\mp} = 12\bar{g}C^W \frac{s}{\Lambda^2}, \quad (\text{A.18})$$

$$\mathcal{M}_{0\pm 0\mp} = \mathcal{M}_{\pm 0\mp 0} = -\frac{3}{4}\bar{g}C^W (3 + \cos\theta) \frac{s}{\Lambda^2} + C^{\varphi W} (1 - \cos\theta) \frac{s}{\Lambda^2}, \quad (\text{A.19})$$

$$\mathcal{M}_{0\pm\mp 0} = \mathcal{M}_{\pm 0 0\mp} = \frac{3}{4}\bar{g}C^W (3 - \cos\theta) \frac{s}{\Lambda^2} - C^{\varphi W} (1 + \cos\theta) \frac{s}{\Lambda^2}, \quad (\text{A.20})$$

$$\mathcal{M}_{0000} = \left(2C^{\varphi\Box} + C^{\varphi D} \right) \frac{s}{\Lambda^2}. \quad (\text{A.21})$$

The SM EFT leading- s contributions from CP-Violating couplings associated to operators in the CPV row in Table 1 are:

$$\mathcal{M}_{++--} = -\mathcal{M}_{--++} = -12\bar{g}C^{\widetilde{W}} \frac{s}{\Lambda^2}, \quad (\text{A.22})$$

$$\begin{aligned} \mathcal{M}_{+---} &= \mathcal{M}_{-+--} = -\mathcal{M}_{--+-} = -\mathcal{M}_{----} = 6\bar{g}C^{\widetilde{W}} \frac{s}{\Lambda^2} \\ &= -\mathcal{M}_{-+++} = -\mathcal{M}_{+-++} = \mathcal{M}_{++-+} = \mathcal{M}_{++++}, \end{aligned} \quad (\text{A.23})$$

$$\begin{aligned} \mathcal{M}_{0+-0} &= \mathcal{M}_{+00-} = -\frac{3}{4}\bar{g}C^{\widetilde{W}} (3 - \cos\theta) \frac{s}{\Lambda^2} + C^{\varphi\widetilde{W}} (1 + \cos\theta) \frac{s}{\Lambda^2} = \\ &= -\mathcal{M}_{0-+0} = -\mathcal{M}_{-00+}, \end{aligned} \quad (\text{A.24})$$

$$\begin{aligned} \mathcal{M}_{0+0-} &= \mathcal{M}_{+0-0} = \frac{3}{4}\bar{g}C^{\widetilde{W}} (3 + \cos\theta) \frac{s}{\Lambda^2} - C^{\varphi\widetilde{W}} (1 - \cos\theta) \frac{s}{\Lambda^2} = \\ &= -\mathcal{M}_{0-0+} = -\mathcal{M}_{-0+0}. \end{aligned} \quad (\text{A.25})$$

The SM results for the amplitudes agree with refs. [38, 82]. We convert the set of parameters $\{\bar{g}, \bar{g}', \bar{v}, \lambda\}$, to a set of input observables¹⁶ $\{G_F, m_W, m_Z, m_h\}$ and write out analytically the cross-sections in the c.m. frame for Longitudinal and Transverse gauge bosons averaging over the initial

¹⁶See for example ref. [83] for the conversion.

helicities. We find at leading order in s :

$$\sigma_{TTTT}(s) = \frac{8}{\pi s} (G_F m_W^2)^2 c \left(\frac{9-c^2}{1-c^2} \right) + \frac{36\sqrt{2}c}{\pi s} (G_F m_W^2) \left(|C^W|^2 + |C^{\widetilde{W}}|^2 \right) \left(\frac{s}{\Lambda^2} \right)^2, \quad (\text{A.26})$$

$$\begin{aligned} \sigma_{LLLL}(s) &= \frac{1}{2\pi s} (G_F m_Z^2)^2 \left[c \frac{9-c^2}{1-c^2} - 2(c+2L_c) \frac{m_h^2}{m_Z^2} + \left(\frac{m_h^2}{m_Z^2} \right)^2 \right] \\ &+ \frac{\sqrt{2}}{4\pi s} (G_F m_Z^2) (2C^{\varphi\Box} + C^{\varphi D}) \left(\frac{s}{\Lambda^2} \right) \left[(c+2L_c) - c \frac{m_h^2}{m_Z^2} \right] \\ &+ \frac{c}{16\pi s} \left(\frac{s}{\Lambda^2} \right)^2 (2C^{\varphi\Box} + C^{\varphi D})^2, \end{aligned} \quad (\text{A.27})$$

$$\begin{aligned} \sigma_{LTLT}(s) &= \sigma_{TLTL}(s) = \sigma_{TLLT}(s) = \sigma_{LTTL}(s) = \frac{8}{\pi s} (G_F m_W)^2 \left(\frac{c}{1-c^2} \right) \\ &- \frac{2^{1/4}}{16\pi s} (G_F m_W^2)^{1/2} \left(\frac{s}{\Lambda^2} \right)^2 c(9-c^2) \Re \left(C^W C^{\varphi W^*} + C^{\widetilde{W}} C^{\varphi \widetilde{W}^*} \right) \\ &+ \frac{3}{16\pi s} \left(\frac{s}{\Lambda^2} \right)^2 \left[\frac{c(3+c^2)}{9} \left(|C^{\varphi W}|^2 + |C^{\varphi \widetilde{W}}|^2 \right) + \frac{\sqrt{2}c(27+c^2)}{4} (G_F m_W^2) \left(|C^W|^2 + |C^{\widetilde{W}}|^2 \right) \right]. \end{aligned} \quad (\text{A.28})$$

Since $\cos\theta \rightarrow 0$ is not attainable we have used a cut at small angle θ_{cut} and integrate over θ_{cut} to $\pi - \theta_{cut}$. In eqs. (A.26)-(A.28) we used the abbreviations: $c \equiv \cos\theta_{cut}$, and $L_c \equiv \log\left(\frac{1-c}{1+c}\right)$. Numerically, if $\theta_{cut} = \pi/18$ then $(1-c^2)^{-1} \approx 33$ and $L_c \approx -5$ and therefore, cross-sections are dominated by angles close to the beam.

A.2 Helicity amplitudes for pure transversal W 's with up to $d = 8$ operators

One of the important outcomes of our analysis is that VBS cross-section is strongly affected by the operator $O_W = \epsilon^{IJK} W_{\mu\rho}^I W^{\rho\sigma,J} W_{\sigma}^{\mu,K}$ which enters in the transverse- W four-point interactions. Since this operator is not affected by Higgs field redefinitions after EW symmetry breaking, the inclusion of pure transverse W^4 operators is straightforward. For pure interactions W^4 the basis for dimension-8 operators reads [16, 17, 48, 49]¹⁷

$$O_{t0} = (W_{\mu\nu}^I W^{\mu\nu,I})(W_{\alpha\beta}^J W^{\alpha\beta,J}), \quad (\text{A.29})$$

$$O_{t1} = (W_{\alpha\nu}^I W^{\mu\beta,I})(W_{\mu\beta}^J W^{\alpha\nu,J}), \quad (\text{A.30})$$

$$O_{t2} = (W_{\alpha\mu}^I W^{\mu\beta,I})(W_{\beta\nu}^J W^{\nu\alpha,J}), \quad (\text{A.31})$$

$$O_{t10} = (W_{\mu\nu}^I \widetilde{W}^{\mu\nu,I})(W_{\alpha\beta}^J \widetilde{W}^{\alpha\beta,J}). \quad (\text{A.32})$$

The *leading-s*, CP-even, helicity amplitudes up to $1/\Lambda^4$, is symbolically written as,

$$\mathcal{M} = \text{SM} + \text{SM} \cdot \text{dim6} + (\text{dim6})^2 + \text{SM} \cdot \text{dim8}, \quad (\text{A.33})$$

¹⁷Our notation for dimension-8 operators follows closely the Warsaw basis article [15] where operators contain only gauge fields and not weighted by gauge couplings. For comparisons, our C^{ti} coefficients are $g^4/4$ times those of Ref. [49].

are found to be

$$\mathcal{M}_{\pm\pm\pm\pm} = -\frac{8\bar{g}^2}{1 - \cos^2\theta} + 4(2C^{t1} + C^{t2})\frac{s^2}{\Lambda^4}, \quad (\text{A.34})$$

$$\begin{aligned} \mathcal{M}_{\pm\mp\pm\mp} &= -2\bar{g}^2\frac{1 + \cos\theta}{1 - \cos\theta} - \frac{9}{2}|C^W|^2\cos^2\left(\frac{\theta}{2}\right)(3 - \cos\theta)\frac{s^2}{\Lambda^4} \\ &+ (\cos\theta + 1)^2(2C^{t0} + C^{t1} + C^{t2} - 2C^{t10})\frac{s^2}{\Lambda^4}, \end{aligned} \quad (\text{A.35})$$

$$\begin{aligned} \mathcal{M}_{\pm\pm\mp\mp} &= 12\bar{g}C^W\frac{s}{\Lambda^2} - \frac{9}{2}(3 - \cos^2\theta)|C^W|^2\frac{s^2}{\Lambda^4} \\ &+ (1 + \cos^2\theta)(4C^{t0} + 2C^{t1} + C^{t2} + 4C^{t10})\frac{s^2}{\Lambda^4} + 8C^{t1}\frac{s^2}{\Lambda^4}, \end{aligned} \quad (\text{A.36})$$

$$\mathcal{M}_{\pm\mp\mp\mp} = -6\bar{g}C^W\frac{s}{\Lambda^2}. \quad (\text{A.37})$$

The multiplicities of the above helicity amplitudes into the transversely polarized cross-section σ_{TTTT} , are 2:4:2:8, respectively. All other contributions not written explicitly in eqs. (A.34)-(A.37), growing at most like (sv^2/Λ^4) , are neglected. It is amusing to note that $(\text{dim}6)^2$ terms do not involve gauge couplings (as they should) in broken phase: they result from the sum of Z and γ tree-diagrams with identical Lorentz structures (see WWZ and $WW\gamma$ vertices in [36]). On the other hand, dimension-8 leading- s contributions arise from contact terms only.

References

- [1] S. Weinberg, *A Model of Leptons*, *Phys.Rev.Lett.* **19** (1967) 1264.
- [2] S. Glashow, *Partial Symmetries of Weak Interactions*, *Nucl.Phys.* **22** (1961) 579.
- [3] A. Salam, *in proceedings of the eighth nobel symposium, edited by n. svartholm (wiley, new york, 1968), p.367., .*
- [4] S. Weinberg, *Effective Gauge Theories*, *Phys. Lett.* **B91** (1980) 51.
- [5] C. G. Callan, Jr., S. R. Coleman, J. Wess and B. Zumino, *Structure of phenomenological Lagrangians. 2.*, *Phys. Rev.* **177** (1969) 2247.
- [6] S. R. Coleman, J. Wess and B. Zumino, *Structure of phenomenological Lagrangians. 1.*, *Phys. Rev.* **177** (1969) 2239.
- [7] D. R. Green, P. Meade and M.-A. Pleier, *Multiboson interactions at the LHC*, *Rev. Mod. Phys.* **89** (2017) 035008 [1610.07572].
- [8] B. Biedermann, A. Denner and M. Pellen, *Large electroweak corrections to vector-boson scattering at the Large Hadron Collider*, *Phys. Rev. Lett.* **118** (2017) 261801 [1611.02951].
- [9] D. Buttazzo, D. Redigolo, F. Sala and A. Tesi, *Fusing Vectors into Scalars at High Energy Lepton Colliders*, *JHEP* **11** (2018) 144 [1807.04743].
- [10] A. Costantini, F. De Lillo, F. Maltoni, L. Mantani, O. Mattelaer, R. Ruiz et al., *Vector boson fusion at multi-TeV muon colliders*, *JHEP* **09** (2020) 080 [2005.10289].

- [11] CMS collaboration, *Measurements of production cross sections of WZ and same-sign WW boson pairs in association with two jets in proton-proton collisions at $\sqrt{s} = 13$ TeV*, *Phys. Lett. B* **809** (2020) 135710 [2005.01173].
- [12] CMS collaboration, *Observation of electroweak production of same-sign W boson pairs in the two jet and two same-sign lepton final state in proton-proton collisions at $\sqrt{s} = 13$ TeV*, *Phys. Rev. Lett.* **120** (2018) 081801 [1709.05822].
- [13] I. Brivio and M. Trott, *The Standard Model as an Effective Field Theory*, *Phys. Rept.* **793** (2019) 1 [1706.08945].
- [14] T. Appelquist and J. Carazzone, *Infrared Singularities and Massive Fields*, *Phys. Rev.* **D11** (1975) 2856.
- [15] B. Grzadkowski, M. Iskrzynski, M. Misiak and J. Rosiek, *Dimension-Six Terms in the Standard Model Lagrangian*, *JHEP* **10** (2010) 085 [1008.4884].
- [16] C. W. Murphy, *Dimension-8 Operators in the Standard Model Effective Field Theory*, 2005.00059.
- [17] H.-L. Li, Z. Ren, J. Shu, M.-L. Xiao, J.-H. Yu and Y.-H. Zheng, *Complete Set of Dimension-8 Operators in the Standard Model Effective Field Theory*, 2005.00008.
- [18] J. Bagger, V. D. Barger, K.-m. Cheung, J. F. Gunion, T. Han, G. A. Ladinsky et al., *The Strongly interacting W W system: Gold plated modes*, *Phys. Rev.* **D49** (1994) 1246 [hep-ph/9306256].
- [19] D. Espriu and B. Yencho, *Longitudinal WW scattering in light of the “Higgs boson” discovery*, *Phys. Rev. D* **87** (2013) 055017 [1212.4158].
- [20] J. Chang, K. Cheung, C.-T. Lu and T.-C. Yuan, *WW scattering in the era of post-Higgs-boson discovery*, *Phys. Rev. D* **87** (2013) 093005 [1303.6335].
- [21] W. Kilian, T. Ohl, J. Reuter and M. Sekulla, *High-Energy Vector Boson Scattering after the Higgs Discovery*, *Phys. Rev. D* **91** (2015) 096007 [1408.6207].
- [22] S. Brass, C. Fleper, W. Kilian, J. Reuter and M. Sekulla, *Transversal Modes and Higgs Bosons in Electroweak Vector-Boson Scattering at the LHC*, *Eur. Phys. J. C* **78** (2018) 931 [1807.02512].
- [23] J. Baglio et al., *VBSCan Mid-Term Scientific Meeting*, in *VBSCan Mid-Term Scientific Meeting*, 4, 2020, 2004.00726.
- [24] C. Degrande, O. Eboli, B. Feigl, B. Jäger, W. Kilian, O. Mattelaer et al., *Monte Carlo tools for studies of non-standard electroweak gauge boson interactions in multi-boson processes: A Snowmass White Paper*, in *Community Summer Study 2013: Snowmass on the Mississippi*, 9, 2013, 1309.7890.
- [25] O. J. P. Éboli and M. C. Gonzalez-Garcia, *Classifying the bosonic quartic couplings*, *Phys. Rev. D* **93** (2016) 093013 [1604.03555].
- [26] M. Fabbrichesi, M. Pinamonti, A. Tonerero and A. Urbano, *Vector boson scattering at the LHC: A study of the WW \rightarrow WW channels with the Warsaw cut*, *Phys. Rev. D* **93** (2016) 015004 [1509.06378].

- [27] R. Gomez-Ambrosio, *Studies of Dimension-Six EFT effects in Vector Boson Scattering*, *Eur. Phys. J.* **C79** (2019) 389 [1809.04189].
- [28] S. Dawson, S. Homiller and S. D. Lane, *Putting SMEFT Fits to Work*, 2007.01296.
- [29] J. Ellis, C. W. Murphy, V. Sanz and T. You, *Updated Global SMEFT Fit to Higgs, Diboson and Electroweak Data*, *JHEP* **06** (2018) 146 [1803.03252].
- [30] O. Domenech, A. Pomarol and J. Serra, *Probing the SM with Dijets at the LHC*, *Phys. Rev. D* **85** (2012) 074030 [1201.6510].
- [31] CMS collaboration, *Search for new physics with dijet angular distributions in proton-proton collisions at $\sqrt{s} = 13$ TeV*, *JHEP* **07** (2017) 013 [1703.09986].
- [32] S. Alte, M. König and W. Shepherd, *Consistent Searches for SMEFT Effects in Non-Resonant Dijet Events*, *JHEP* **01** (2018) 094 [1711.07484].
- [33] A. Falkowski, M. Gonzalez-Alonso, A. Greljo, D. Marzocca and M. Son, *Anomalous Triple Gauge Couplings in the Effective Field Theory Approach at the LHC*, *JHEP* **02** (2017) 115 [1609.06312].
- [34] ATLAS collaboration, *Observation of electroweak production of a same-sign W boson pair in association with two jets in pp collisions at $\sqrt{s} = 13$ TeV with the ATLAS detector*, 1906.03203.
- [35] ATLAS collaboration, *Observation of electroweak $W^\pm Z$ boson pair production in association with two jets in pp collisions at $\sqrt{s} = 13$ TeV with the ATLAS detector*, *Phys. Lett.* **B793** (2019) 469 [1812.09740].
- [36] A. Dedes, W. Materkowska, M. Paraskevas, J. Rosiek and K. Suxho, *Feynman rules for the Standard Model Effective Field Theory in R_ξ -gauges*, *JHEP* **06** (2017) 143 [1704.03888].
- [37] J. M. Cornwall, D. N. Levin and G. Tiktopoulos, *Derivation of Gauge Invariance from High-Energy Unitarity Bounds on the s Matrix*, *Phys. Rev.* **D10** (1974) 1145.
- [38] C. E. Vayonakis, *Born Helicity Amplitudes and Cross-Sections in Nonabelian Gauge Theories*, *Lett. Nuovo Cim.* **17** (1976) 383.
- [39] B. W. Lee, C. Quigg and H. B. Thacker, *Weak Interactions at Very High-Energies: The Role of the Higgs Boson Mass*, *Phys. Rev.* **D16** (1977) 1519.
- [40] M. S. Chanowitz and M. K. Gaillard, *The TeV Physics of Strongly Interacting W 's and Z 's*, *Nucl. Phys.* **B261** (1985) 379.
- [41] G. J. Gounaris, R. Kogerler and H. Neufeld, *Relationship Between Longitudinally Polarized Vector Bosons and their Unphysical Scalar Partners*, *Phys. Rev.* **D34** (1986) 3257.
- [42] Y.-P. Yao and C. P. Yuan, *Modification of the Equivalence Theorem Due to Loop Corrections*, *Phys. Rev.* **D38** (1988) 2237.
- [43] J. Bagger and C. Schmidt, *Equivalence Theorem Redux*, *Phys. Rev.* **D41** (1990) 264.
- [44] C. Arzt, M. B. Einhorn and J. Wudka, *Patterns of deviation from the standard model*, *Nucl. Phys.* **B433** (1995) 41 [hep-ph/9405214].

- [45] B. Gavela, E. Jenkins, A. Manohar and L. Merlo, *Analysis of General Power Counting Rules in Effective Field Theory*, *Eur. Phys. J. C* **76** (2016) 485 [1601.07551].
- [46] D. Liu, A. Pomarol, R. Rattazzi and F. Riva, *Patterns of Strong Coupling for LHC Searches*, *JHEP* **11** (2016) 141 [1603.03064].
- [47] A. Azatov, R. Contino, C. S. Machado and F. Riva, *Helicity selection rules and noninterference for BSM amplitudes*, *Phys. Rev.* **D95** (2017) 065014 [1607.05236].
- [48] G. N. Remmen and N. L. Rodd, *Consistency of the Standard Model Effective Field Theory*, *JHEP* **12** (2019) 032 [1908.09845].
- [49] K. Yamashita, C. Zhang and S.-Y. Zhou, *Elastic positivity vs extremal positivity bounds in SMEFT: a case study in transversal electroweak gauge-boson scatterings*, 2009.04490.
- [50] C. de Rham, S. Melville, A. J. Tolley and S.-Y. Zhou, *UV complete me: Positivity Bounds for Particles with Spin*, *JHEP* **03** (2018) 011 [1706.02712].
- [51] J. Ellis, H.-J. He and R.-Q. Xiao, *Probing New Physics in Dimension-8 Neutral Gauge Couplings at e^+e^- Colliders*, 2008.04298.
- [52] J. de Blas, J. Criado, M. Perez-Victoria and J. Santiago, *Effective description of general extensions of the Standard Model: the complete tree-level dictionary*, *JHEP* **03** (2018) 109 [1711.10391].
- [53] D. Marzocca et al., *BSM Benchmarks for Effective Field Theories in Higgs and Electroweak Physics*, 2009.01249.
- [54] G. Chaudhary, J. Kalinowski, M. Kaur, P. Kozów, K. Sandeep, M. Szeleper et al., *EFT triangles in the same-sign WW scattering process at the HL-LHC and HE-LHC*, *Eur. Phys. J. C* **80** (2020) 181 [1906.10769].
- [55] J. Kalinowski, P. Kozów, S. Pokorski, J. Rosiek, M. Szeleper and S. Tkaczyk, *Same-sign WW scattering at the LHC: can we discover BSM effects before discovering new states?*, *Eur. Phys. J. C* **78** (2018) 403 [1802.02366].
- [56] C. Garcia-Garcia, M. Herrero and R. A. Morales, *Unitarization effects in EFT predictions of WZ scattering at the LHC*, *Phys. Rev. D* **100** (2019) 096003 [1907.06668].
- [57] M. Jacob and G. C. Wick, *On the General Theory of Collisions for Particles with Spin*, *Annals Phys.* **7** (1959) 404.
- [58] V. D. Barger, K.-m. Cheung, T. Han and R. J. N. Phillips, *Strong W^+W^+ scattering signals at pp supercolliders*, *Phys. Rev. D* **42** (1990) 3052.
- [59] P. Chankowski, *Lecture notes: "QFT as a theory of particles - S-matrix and the scattering theory fuw.edu.pl/[tilde]chank/qftoei.html*, .
- [60] P. Kozów, *The W and Z scattering as a probe of physics beyond the Standard Model: Effective Field Theory approach*, Ph.D. thesis, Warsaw U., 2019. 1908.07596.
- [61] K. Arnold et al., *VBFNLO: A Parton level Monte Carlo for processes with electroweak bosons*, *Comput. Phys. Commun.* **180** (2009) 1661 [0811.4559].

- [62] T. Corbett, O. J. P. Éboli and M. C. Gonzalez-Garcia, *Unitarity Constraints on Dimension-Six Operators*, *Phys. Rev.* **D91** (2015) 035014 [1411.5026].
- [63] E. d. S. Almeida, O. Éboli and M. Gonzalez-Garcia, *Unitarity constraints on anomalous quartic couplings*, *Phys. Rev. D* **101** (2020) 113003 [2004.05174].
- [64] M. Froissart, *Asymptotic behavior and subtractions in the mandelstam representation*, *Phys. Rev.* **123** (1961) 1053.
- [65] J. Alwall, R. Frederix, S. Frixione, V. Hirschi, F. Maltoni, O. Mattelaer et al., *The automated computation of tree-level and next-to-leading order differential cross sections, and their matching to parton shower simulations*, *JHEP* **07** (2014) 079 [1405.0301].
- [66] A. Dedes, M. Paraskevas, J. Rosiek, K. Suxho and L. Trifyllis, *SmeftFR – Feynman rules generator for the Standard Model Effective Field Theory*, 1904.03204.
- [67] A. Alloul, N. D. Christensen, C. Degrande, C. Duhr and B. Fuks, *FeynRules 2.0 - A complete toolbox for tree-level phenomenology*, *Comput. Phys. Commun.* **185** (2014) 2250 [1310.1921].
- [68] C. Degrande, C. Duhr, B. Fuks, D. Grellscheid, O. Mattelaer and T. Reiter, *UFO - The Universal FeynRules Output*, *Comput. Phys. Commun.* **183** (2012) 1201 [1108.2040].
- [69] T. Sjostrand, S. Mrenna and P. Z. Skands, *PYTHIA 6.4 Physics and Manual*, *JHEP* **05** (2006) 026 [hep-ph/0603175].
- [70] T. Sjostrand, S. Mrenna and P. Z. Skands, *A Brief Introduction to PYTHIA 8.1*, *Comput. Phys. Commun.* **178** (2008) 852 [0710.3820].
- [71] E. Conte, B. Fuks and G. Serret, *MadAnalysis 5, A User-Friendly Framework for Collider Phenomenology*, *Comput. Phys. Commun.* **184** (2013) 222 [1206.1599].
- [72] M. Cacciari, G. P. Salam and G. Soyez, *FastJet User Manual*, *Eur. Phys. J. C* **72** (2012) 1896 [1111.6097].
- [73] A. Falkowski, *Higgs Basis: Proposal for an EFT basis choice for LHC HXSWG*, <http://cds.cern.ch/record/2001958?ln=pl>.
- [74] A. Ballestrero, E. Maina and G. Pelliccioli, *W boson polarization in vector boson scattering at the LHC*, *JHEP* **03** (2018) 170 [1710.09339].
- [75] A. Ballestrero, E. Maina and G. Pelliccioli, *Different polarization definitions in same-sign WW scattering at the LHC*, 2007.07133.
- [76] F. Krauss, S. Kuttimalai and T. Plehn, *LHC multijet events as a probe for anomalous dimension-six gluon interactions*, *Phys. Rev. D* **95** (2017) 035024 [1611.00767].
- [77] A. Falkowski and D. Straub, *Flavourful SMEFT likelihood for Higgs and electroweak data*, *JHEP* **04** (2020) 066 [1911.07866].
- [78] P. Kozów, L. Merlo, S. Pokorski and M. Szleper, *Same-sign WW Scattering in the HEFT: Discoverability vs. EFT Validity*, *JHEP* **07** (2019) 021 [1905.03354].
- [79] A. Denner and T. Hahn, *Radiative corrections to $W^+W^- \rightarrow W^+W^-$ in the electroweak standard model*, *Nucl. Phys.* **B525** (1998) 27 [hep-ph/9711302].

- [80] T. Hahn, *Generating Feynman diagrams and amplitudes with FeynArts 3*, *Comput. Phys. Commun.* **140** (2001) 418 [[hep-ph/0012260](#)].
- [81] T. Hahn and M. Perez-Victoria, *Automatized one loop calculations in four-dimensions and D-dimensions*, *Comput. Phys. Commun.* **118** (1999) 153 [[hep-ph/9807565](#)].
- [82] J. Layssac, F. M. Renard and G. J. Gounaris, *Vector boson pair production at supercollider: Useful approximate helicity amplitudes*, *Z. Phys.* **C62** (1994) 139 [[hep-ph/9309324](#)].
- [83] A. Dedes, K. Suxho and L. Trifyllis, *The decay $h \rightarrow Z\gamma$ in the Standard-Model Effective Field Theory*, *JHEP* **06** (2019) 115 [[1903.12046](#)].